

New Intrinsic Fast Scintillator: Cesium Praseodymium Chloride

Yutaka Fujimoto,^{1*} Daisuke Nakauchi,² Takayuki Yanagida,²
Masanori Koshimizu,¹ and Keisuke Asai¹

¹Department of Applied Chemistry, Graduate School of Engineering, Tohoku University, Sendai 980-8579, Japan

²Graduate School of Materials Science, Nara Institute of Science and Technology,
8916-5 Takayama, Ikoma, Nara 630-0192, Japan

(Received October 15, 2021; accepted October 28, 2021)

Keywords: scintillator, chloride, Pr³⁺ 5d–4f transitions

A sample of Cs₃PrCl₆ crystal was grown under vacuum using the vertical Bridgman–Stockbarger method. The excitation spectrum, monitored at an emission wavelength of 310 nm, showed at least two excitation bands at around 233 and 257 nm. These excitation bands corresponded to the transitions from 4f² ground states (³H_J and ³F_J) to 5d excited states of Pr³⁺ split by the ligand-field interaction and the spin-orbit coupling. Upon UV excitation at 233 nm, the characteristic Pr³⁺ 4f¹5d¹→4f² emission bands were observed at 285 and 312 nm. The scintillation spectrum shows two emission bands peaking at 285 and 312 nm, which is consistent with the photoluminescence, and can thus be assigned to the transitions between the 5d¹ excited state and 4f² ground states owing to the Pr³⁺. The fast scintillation decay time constants were estimated to be approximately 11.7 ns (53%) and 72 ns (47%). The scintillation light yield reached 5900 ph/MeV.

1. Introduction

Scintillation materials play a central role in the detection and measurement of ionizing radiation such as X-rays and gamma rays as they provide an efficient means of converting high-energy electromagnetic radiation into UV-visible light that can be detected with photosensitive sensors. For the development of a scintillation detector with good coincidence timing and high count-rate capability, a scintillator with a combination of high light yield and short decay time is strongly required. Cerium-doped crystalline scintillators such as Gd₂SiO₅:Ce, (Lu, Y)₂SiO₅:Ce, and (Lu, Gd)₂SiO₅:Ce,^(1–4) are now available for use as radiation detectors in time-of-flight position emission tomography (TOF-PET)^(5–7) because of their many advantages, which are a high light output of more than 10000 ph/MeV, a short decay time of several tens of nanoseconds due to the 5d–4f electric-dipole parity-allowed transitions of Ce³⁺, and the capability of obtaining large crystals. Owing to its success in medical applications, the Ce³⁺ ion has become a well-known emission center in the field of developing scintillator materials.^(8–17) Some researchers are currently focusing on Ce-concentrated ternary chloride scintillators because of the large atomic number of Ce (Z = 58), as well as their high light yields and short decay times due to the

*Corresponding author: e-mail: fuji-you@qpc.che.tohoku.ac.jp
<https://doi.org/10.18494/SAM3693>

5d–4f allowed transitions of Ce^{3+} .^(18–21) Meanwhile, most common scintillators activated by extrinsic dopants tend to have an inhomogeneous dopant distribution in the crystal. The above self-activated scintillators have the potential to exhibit uniform quality and characteristics. In 2007, K_2CeCl_5 was first introduced as a scintillator by Roy *et al.*⁽¹⁸⁾ The K_2CeCl_5 crystal shows a high light yield of 30000 ph/MeV with an energy resolution of 5.8% at 662 keV and is much less hygroscopic than LaBr_3 . After 2011, CsCl–CeCl_3 -based ternary scintillators such as Cs_3CeCl_6 and CsCe_2Cl_7 were intensely studied by Zhuravleva *et al.*⁽²⁰⁾ For their crystals, the light yield reached ~ 26000 ph/MeV with a fast principal decay time of 50 ns. These Ce-concentrated halides are very interesting because of their low concentration quenching despite a high Ce concentration compared with Ce^{3+} -doped oxides and other compounds. Thus, in this study, we focused on new CsCl–PrCl_3 -based ternary compounds and investigated a Cs_3PrCl_6 crystalline scintillator. Many researchers have reported that Pr^{3+} -doped crystalline scintillators also exhibit $4f^15d^1 \rightarrow 4f^2$ ($^3\text{H}_J$, $^3\text{F}_J$) allowed transitions and can be an attractive alternative for TOF-PET applications.^(21–25) The Pr^{3+} $4f^15d^1 \rightarrow 4f^2$ emission is caused by a high crystal field strength that shifts the lowest $5d^1$ state of Pr^{3+} below the $^1\text{S}_0$ state of the ground $4f^2$ electronic configuration. A previous study on the decay times of Ce^{3+} and Pr^{3+} in the same compounds such as garnet and perovskite crystals revealed that the decay time of Pr^{3+} is about half that of Ce^{3+} . Here, in an attempt to study Pr-concentrated fast halide scintillators, we report results of the crystal growth, powder X-ray diffraction (PXRD) pattern analysis, photoluminescence (PL), and scintillation property measurements of Cs_3PrCl_6 .

2. Methods

The synthesis procedure of Cs_3PrCl_6 consisted of mixing stoichiometric amounts of CsCl (4N) and PrCl_3 (4N) raw materials into a quartz ampoule and then heating at 350 °C in vacuum for 24 h before crystal growth. After that, the quartz ampoule was sealed under vacuum with an oxygen propane burner torch. The Cs_3PrCl_6 crystal was grown in a two-zone furnace at a temperature gradient of 1.3 °C/mm using a vertical Bridgman furnace (TBR-30V, TECHNO SEARCH CORP.). The temperatures of the upper and lower zones in the vertical furnace were 900 and 700 °C, respectively, where the former is higher than the melting point of Cs_3PrCl_6 (~ 820 °C). After maintaining the furnace temperature for 12 h, the crystal growth was carried out at a growth rate of 1.0 mm/h, then the crystal was cooled to room temperature over several hours at the end of the crystal growth process. To confirm the crystalline phase, PXRD pattern analysis was performed in the 2θ range from 10 to 80° using an Ultima IV diffractometer (RIGAKU) with an X-ray source operated at 40 kV and 40 mA with a copper target. The measurement was carried out on the sample in an air-sensitive holder, which protected the sample from decomposition in ambient air. To understand the luminescence mechanism, PL spectra and PL decay time profile measurements were performed. The excitation and emission spectra were measured using a Hitachi F-7000 fluorescence spectrophotometer equipped with a monochromator and a xenon arc lamp as the excitation source. The PL decay time profile was recorded using a DeltaFlex time-correlated single-photon counting device system (TCSPC, HORIBA). The sample was excited at 250 nm using a pulsed nano-LED excitation source, and the PL photons from the sample were counted using a picosecond photon detection (PPD)-850

module. The scintillation spectrum was measured at room temperature under continuous irradiation from a copper target acting as an X-ray source (SA-HFM3, Rigaku) at power settings of 40 kV and 40 mA. The scintillation light from the sample was detected with a SILVER-Nova multichannel spectrometer (Stellarnet Inc.) that was cooled to $-15\text{ }^{\circ}\text{C}$ using a Peltier module. The sample was optically coupled to an optical fiber head using optical grease, and Teflon tape was used as a reflector to increase the collection of light from diffuse reflections. The scintillation decay time profile was recorded using our original setup with a pulsed-X-ray-induced afterglow characterization system (Hamamatsu Photonics).⁽²⁶⁾ The main modules of the system were an R7400P-06 photomultiplier tube (PMT; Hamamatsu Photonics) and an X-ray tube (N5084, Hamamatsu Photonics) controlled by a picosecond laser diode (PLP10-063, Hamamatsu). Scintillation pulse height spectra under the irradiation of 662 keV gamma rays from a ^{137}Cs source were measured using the sample optically coupled to an R7600U-200 PMT (Hamamatsu Photonics). A detailed explanation of the experimental setup can be found in our previous paper.⁽²⁷⁾ The spectra were recorded with shaping times of $0.5\text{ }\mu\text{s}$ for Cs_3PrCl_6 and $2\text{ }\mu\text{s}$ for $\text{Bi}_4\text{Ge}_3\text{O}_{12}$ (BGO; light yield = $\sim 8600\text{ ph/MeV}$),⁽²⁸⁾ where the latter was used as a standard sample to calculate the scintillation light yield.

3. Results and Discussion

A photograph of the as-grown Cs_3PrCl_6 crystal is shown in Fig. 1(a). The crystal was slightly translucent with a greenish yellow color. The color is due to strong absorption bands in the UV wavelength region, which are caused by electron transitions of Pr^{3+} . Part of the as-grown crystal was cut with a diamond-coated metal wire saw and polished optically to dimensions of $3.0 \times 3.0 \times 1.0\text{ mm}^3$ for PL and scintillation measurements. The PXRD patterns of the grown crystal are shown in Fig. 1(b). The Cs_3PrCl_6 melts congruently at $\sim 830\text{ }^{\circ}\text{C}$ and undergoes a solid–solid phase transition at $\sim 395\text{ }^{\circ}\text{C}$ from cubic (elpasolite-type) to monoclinic (Cs_3BiCl_6 -type) with decreasing temperature.⁽²⁹⁾ The translucency of the crystal may be due to the solid–solid phase

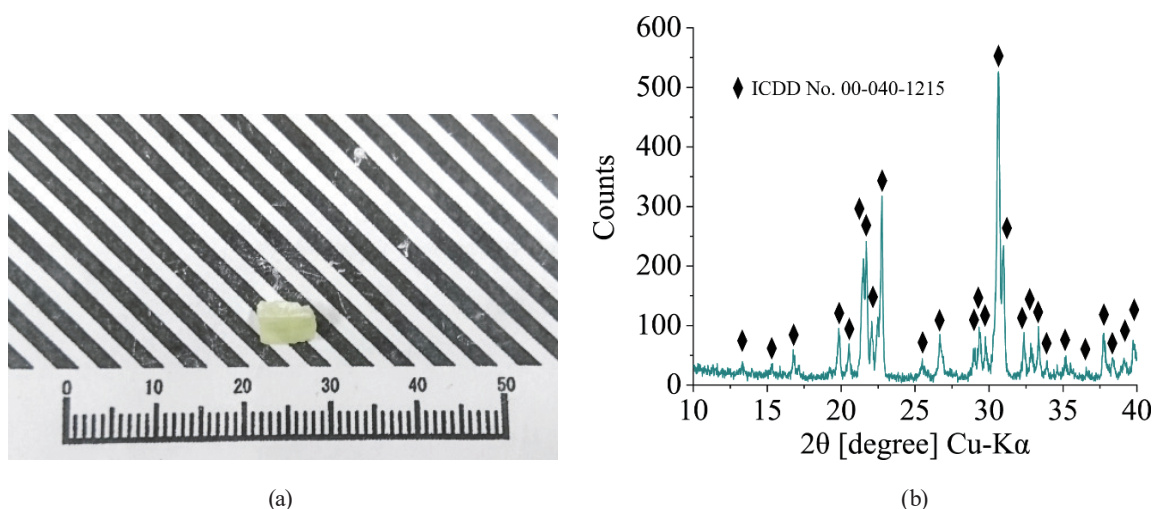


Fig. 1. (Color online) (a) Photograph of as-grown Cs_3PrCl_6 crystal and (b) PXRD patterns of the grown crystal.

transition during crystal growth, as previously reported for a Cs_3CeCl_6 crystal.⁽²⁰⁾ From the phase and crystal structure analyses, the PXRD pattern of the grown crystal is in good agreement with that of the monoclinic Cs_3PrCl_6 structure (ICDD No. 00-040-1215); therefore, it was concluded that we successfully grew a single-phase crystal of Cs_3PrCl_6 without precipitation of the cubic phase. Also, the refined monoclinic unit cell parameters were $a = 14.08 \text{ \AA}$, $b = 8.267 \text{ \AA}$, $c = 13.34 \text{ \AA}$, and $\beta = 108.04^\circ$.

PL excitation and emission spectra of Cs_3PrCl_6 are shown in Fig. 2. The emission spectrum excited at 233 nm shows two peaks at 285 and 312 nm, which are characteristic $\text{Pr}^{3+} 4f^15d^1 \rightarrow 4f^2$ ($^3\text{H}_J$, $^3\text{F}_J$) emission. A weak shoulder band at around 340–400 nm may be due to allowed transitions from the $4f^15d^1$ excited state to the $4f^2$ ($^1\text{G}_4$) state. The excitation spectrum with an emission wavelength of 285 nm shows a major excitation band at 233 nm with a shoulder band at 257 nm. These excitation bands correspond to the transitions from the $4f^2$ ground state to $5d$ excited states of Pr^{3+} . Srivastava reported the relationship between the energy of the $\text{Pr}^{3+} 4f^2 \rightarrow 4f^15d^1$ configuration, Stokes shift, and $^1\text{S}_0$ level for some Pr^{3+} -activated compounds.^(30,31) His report provided evidence that when the Stokes shift of the $\text{Pr}^{3+} 4f^15d^1 \rightarrow 4f^2$ emission is less than about 3000 cm^{-1} , the compounds predominantly show UV emission via the $4f^15d^1 \rightarrow 4f^2$ transition of Pr^{3+} . From the spectra for Cs_3PrCl_6 , the energy of the lowest $\text{Pr}^{3+} 4f^2 \rightarrow 4f^15d^1$ excitation transition and the Stokes shift can be calculated to be approximately 38462 and 1425 cm^{-1} , respectively. Thus, our results are in good agreement with the previous report because Cs_3PrCl_6 shows an intense emission band owing to the $4f^15d^1 \rightarrow 4f^2$ transition of Pr^{3+} , whereas no $4f^2 \rightarrow 4f^2$ transitions of Pr^{3+} can be confirmed in the PL spectra. The PL decay curve of Cs_3PrCl_6 was measured at room temperature, as shown in Fig. 3. Here, the monitoring emission wavelength was 285 nm under excitation by a 250 nm LED. The decay time was obtained by exponential decay fitting after deconvolution of the instrument response function. From the fitting calculation, the decay time of the $\text{Pr}^{3+} 4f^15d^1 \rightarrow 4f^2$ luminescence was found to be approximately 19 ns, which is a comparably fast response to other Pr^{3+} -activated compounds.^(21–25)

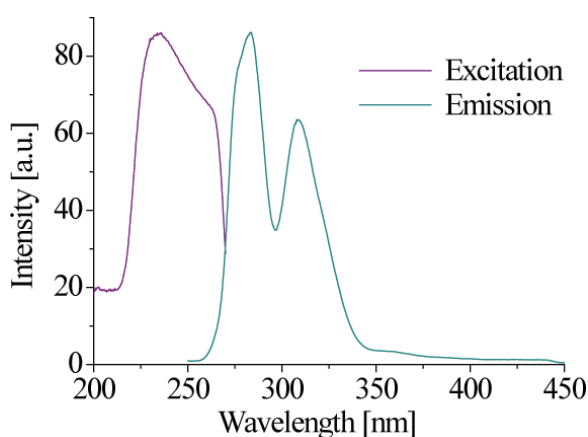


Fig. 2. (Color online) PL excitation (purple line) and emission (green line) spectra of Cs_3PrCl_6 ($\lambda_{em} = 285 \text{ nm}$, $\lambda_{ex} = 233 \text{ nm}$).

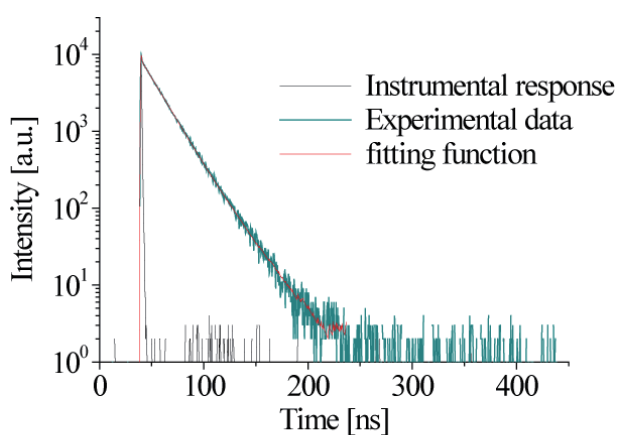


Fig. 3. (Color online) PL decay curve of Cs_3PrCl_6 ($\lambda_{em} = 285 \text{ nm}$, $\lambda_{ex} = 250 \text{ nm}$).

The scintillation spectrum of Cs_3PrCl_6 is shown in Fig. 4. The spectrum is dominated by UV emission bands peaking at 285 and 312 nm. Considering the PL measurements, the two emission peaks at 285 and 312 nm are assigned to transitions from the lowest $4f^15d^1$ excited state to the $4f^2$ ($^3\text{H}_J$, $^3\text{F}_J$) ground state of Pr^{3+} . Also, the weak shoulder band at around 340–400 nm can be assigned to transitions from the $4f^15d^1$ excited state to the $4f^2$ ($^1\text{G}_4$) state. Meanwhile, various types of intrinsic emission such as self-trapped exciton (STE) and core-valence (CV) luminescence have been observed in many cesium-based ternary compounds.^(32–35) In this study, Cs_3PrCl_6 showed no emission band other than the Pr^{3+} emission. Determining the reason for these emission properties is beyond the scope of our present study, although we speculate that the type of emission strongly depends on the electronic band structure and intrinsic optical self-absorption of the compounds. Figure 5 shows the scintillation decay time profile of Cs_3PrCl_6 . The profile was fitted with three exponential decay functions. The calculated decay times were 1.5, 11.7, and 72 ns. The initial fast decay component of 1.5 ns was due to an instrumental response function, whereas the other components were due to the scintillation from the sample. The major decay time constant was 11.7 ns (53%), which is slightly shorter than that of the PL (~19 ns). The mechanism of the accelerated decay time under X-ray excitation has not yet been revealed. Pédrini *et al.* reported and discussed a similar acceleration of the decay time in the CeF_3 crystal.⁽³⁶⁾ According to their study, one possibility is that the acceleration is caused by the creation of quenchers, such as other Pr^{3+} emission centers, near the Pr^{3+} emission centers under X-ray excitation because of the high concentration of Pr^{3+} . The other decay time constant of 72 ns (47%) is longer than that of the PL, which may be due to a complex energy transfer process from the host crystal lattice to the emission centers, in common with some intrinsic scintillators reported previously.^(11,37–39)

The pulse height spectra of Cs_3PrCl_6 and the BGO reference are shown in Fig. 6. The scintillation light yield for Cs_3PrCl_6 was calculated to be approximately 5900 ph/MeV after taking into account the determined 662 keV gamma-ray photo-peak channel, the gain value, and the quantum efficiency of the PMT for the scintillation wavelength of each sample. Compared with commercial fast scintillators such as BaF_2 , CeF_3 , $\text{Gd}_2\text{SiO}_5\text{:Ce}$, and $(\text{Lu}, \text{Y})_2\text{SiO}_5\text{:Ce}$,

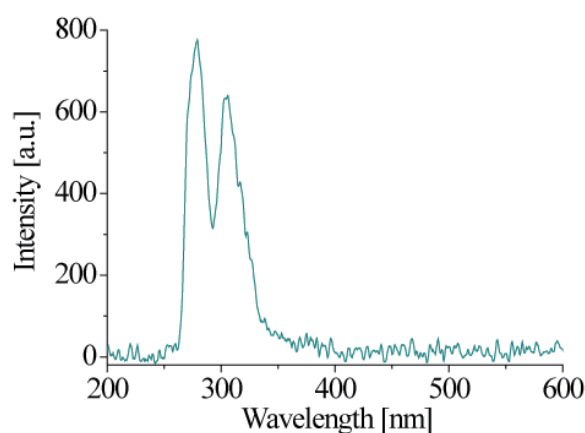


Fig. 4. (Color online) X-ray-excited scintillation spectrum of Cs_3PrCl_6 .

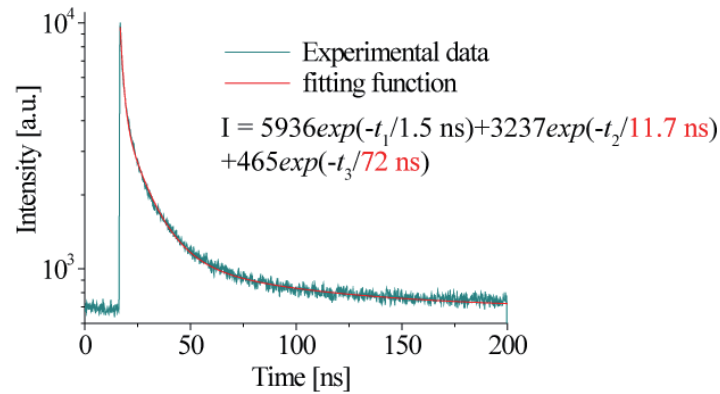


Fig. 5. (Color online) Pulsed X-ray-excited scintillation decay time profile of Cs_3PrCl_6 .

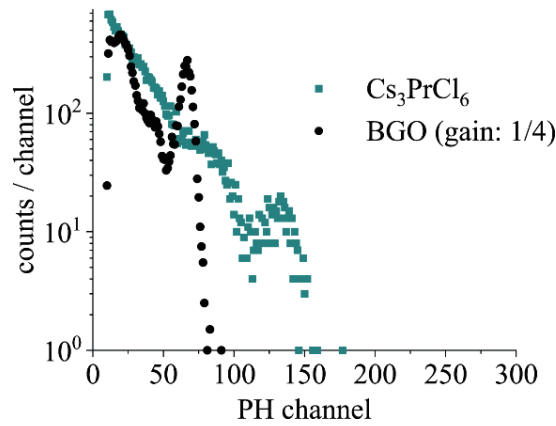


Fig. 6. (Color online) ^{137}Cs -gamma-ray-induced scintillation pulse height spectra of the Cs_3PrCl_6 crystal and a reference BGO commercial scintillator.

Table 1

Characteristics of Cs_3PrCl_6 compared with commercially available BaF_2 , CeF_3 , $\text{Gd}_2\text{SiO}_5:\text{Ce}$, and $(\text{Lu}, \text{Y})_2\text{SiO}_5:\text{Ce}$. (40–42)

	Scintillation wavelength (nm)	Decay time (ns)	Light yield (ph/MeV)
BaF_2	220, 310	0.6 (220 nm), 620 (310 nm)	2500 (220 nm), 7500 (310 nm)
CeF_3	340	27	4300
$\text{Gd}_2\text{SiO}_5:\text{Ce}$	440	60, 600	~9000
$(\text{Lu}, \text{Y})_2\text{SiO}_5:\text{Ce}$	420	40	25000
Cs_3PrCl_6	280–320	11.7 (53%), 72 (47%)	5900

Cs_3PrCl_6 is found to have moderate light yield with a short decay time and a suitable scintillation wavelength for the PMT (see Table 1). The energy resolution at 662 keV was estimated to be approximately ~26%. Upon future refinement of the crystal growth technique, we expect that the light yield and energy resolution will be further improved.

4. Summary

In this work, we present a new intrinsic fast scintillator: Cs₃PrCl₆. A Cs₃PrCl₆ crystal was grown by the vertical Bridgman–Stockbarger technique and its PL and scintillation properties were characterized at room temperature. Under both UV light and X-ray excitation, the crystal showed characteristic Pr³⁺ 4f¹5d¹-4f² emission bands peaking at 285 and 312 nm, which are detectable emission for a common PMT. The scintillation decay consists of two exponential components: a fast component of 11.7 ns (53%) and a slow component of 72 ns (47%). The scintillation light yield is calculated to be approximately 5900 ph/MeV. These attractive performances make this crystal promising for X-ray and gamma-ray detection applications requiring good coincidence timing and a high count-rate capability.

Acknowledgments

This work was supported by the Cooperative Research Project of the Research Center for Biomedical Engineering and Terumo Life Science Foundation.

References

- 1 K. Takagi and T. Fukazawa: *Appl. Phys. Lett.* **42** (1983) 43.
- 2 D. W. Cooke, K. J. McClellan, B. L. Bennett, J. M. Roper, M. T. Whittaker, and R. E. Muenchausen: *J. Appl. Phys.* **88** (2000) 7360.
- 3 G. B. Loutts, A. I. Zagumennyi, S. V. Lavrishehev, Y. D. Zavartsev, and P. A. Studenikin: *J. Cryst. Growth* **174** (1997) 331.
- 4 Y. Fujimoto, D. Nakauchi, T. Yanagida, M. Koshimizu, and K. Asai: *Sens. Mater.* **33** (2021) 2147.
- 5 C. W. E. van Eijk: *Radiat. Prot. Dosim.* **129** (2008) 13.
- 6 C. L. Melcher: *J. Nucl. Med.* **41** (2000) 1051.
- 7 P. Lecoq: *Nucl. Instrum. Methods Phys. Res., Sect. A* **809** (2016) 130.
- 8 E. Zych, C. Brecher, A. J. Wojtowicz, and H. Lingertat: *J. Lumin.* **75** (1997) 193.
- 9 E. V. D. van Loef, P. Dorenbos, and C. W. E. van Eijk: *Appl. Phys. Lett.* **79** (2001) 1573.
- 10 T. Yanagida, K. Kamada, Y. Fujimoto, H. Yagi, and T. Yanagitani: *Opt. Mater.* **35** (2013) 2480.
- 11 Y. Fujimoto, K. Saeki, D. Nakauchi, T. Yanagida, M. Koshimizu, and K. Asai: *Sens. Mater.* **29** (2017) 1425.
- 12 G. Okada, M. Akatsuka, H. Kimura, M. Mori, N. Kawano, N. Kawaguchi, and T. Yanagida: *Sens. Mater.* **30** (2018) 1547.
- 13 A. Khan, G. Rooh, H. J. Kim, and S. Kim: *J. Alloys Compd.* **741** (2018) 878.
- 14 H. Kimura, F. Nakamura, T. Kato, D. Nakauchi, G. Okada, N. Kawaguchi, and T. Yanagida: *Sens. Mater.* **30** (2018) 1555.
- 15 H. Fukushima, D. Nakauchi, N. Kawaguchi, and T. Yanagida: *Sens. Mater.* **31** (2019) 1273.
- 16 U. Shirwadkar, M. Loyd, M. H. Du, E. V. Loef, G. Ciampi, L. S. Pandian, L. Stand, M. Koschan, M. Zhuravleva, C. Melcher, and K. Shah: *Nucl. Instrum. Methods Phys. Res., Sect. A* **962** (2020) 163684.
- 17 S. Matsumoto, A. Minamino, and A. Ito: *Sens. Mater.* **33** (2021) 2209.
- 18 U. N. Roy, M. Groza, Y. Cui, A. Burger, N. Cherepy, S. Friedrich, and S. A. Payne: *Nucl. Instrum. Methods Phys. Res., Sect. A* **579** (2007) 46.
- 19 R. Hawrami, A. K. Batra, M. D. Aggarwal, U. N. Roy, M. Groza, Y. Cui, A. Burger, N. Cherepy, T. Niedermayr, and S. A. Payne: *J. Cryst. Growth* **310** (2008) 2099.
- 20 M. Zhuravleva, K. Yang, and C. L. Melcher: *J. Cryst. Growth* **318** (2011) 809.
- 21 Y. Fujimoto, K. Saeki, D. Nakauchi, T. Yanagida, M. Koshimizu, and K. Asai: *Sens. Mater.* **31** (2019) 1241.
- 22 M. Nikl, H. Ogino, A. Krasnikov, A. Beitlerova, A. Yoshikawa, and T. Fukuda: *Phys. Status Solidi A* **202** (2005) R4.
- 23 W. Drozdowski, T. Lukasiewicz, A. J. Wojtowicz, D. Wisniewski, and J. Kisielewski: *J. Cryst. Growth* **275** (2005) e709.

- 24 T. Yanagida, A. Yoshikawa, Y. Yokota, K. Kamada, Y. Usuki, S. Yamamoto, M. Miyake, M. Baba, K. Kumagai, K. Sasaki, M. Ito, N. Abe, Y. Fujimoto, S. Maeo, Y. Furuya, H. Tanaka, A. Fukabori, T. R. dos Santos, M. Takeda, and N. Ohuchi: *IEEE Trans. Nucl. Sci.* **57** (2010) 1492.
- 25 P. Kantuptim, M. Akatsuka, D. Nakauchi, T. Kato, N. Kawaguchi, and T. Yanagida: *Sens. Mater.* **32** (2020) 1357.
- 26 T. Yanagida, Y. Fujimoto, T. Ito, K. Uchiyama, and K. Mori: *Appl. Phys. Exp.* **7** (2014) 062401.
- 27 T. Yanagida, Y. Fujimoto, H. Yagi, and T. Yanagitani: *Opt. Mater.* **36** (2014) 1044.
- 28 M. Moszynski, M. Kapusta, M. Mayhugh, D. Wolski, and S. O. Flyckt: *IEEE Trans. Nucl. Sci.* **44** (1997) 1052.
- 29 L. Rycerz and M. G. Escard: Correlation between Thermodynamic Properties, Electrical Conductivity and Crystal Structure of M3LnX6 Compounds Molten Salts and Technology Conference Paper (2008).
- 30 A. M. Srivastava: *J. Lumi.* **169** (2016) 445.
- 31 A. M. Srivastava, M. Jennings, and J. Collins: *Opt. Mater.* **34** (2012) 1347.
- 32 M. Koshimizu, N. Yahaba, R. Haruki, F. Nishikido, S. Kishimoto, and K. Asai: *Opt. Mater.* **36** (2014) 1930.
- 33 N. Yahaba, M. Koshimizu, Y. Sun, T. Yanagida, Y. Fujimoto, R. Haruki, F. Nishikido, S. Kishimoto, and K. Asai: *Appl. Phys. Express* **7** (2014) 062602.
- 34 T. Sakai, M. Koshimizu, Y. Fujimoto, D. Nakauchi, T. Yanagida, and K. Asai: *Sens. Mater.* **30** (2018) 1565.
- 35 K. Takahashi, M. Koshimizu, Y. Fujimoto, T. Yanagida, and K. Asai: *Nucl. Instrum. Methods Phys. Res., Sect. A* **954** (2020) 161842.
- 36 C. Pédrini, A. Belsky, and B. M. D. Buttet: *Acta Phys. Pol. A* **84** (1993) 953.
- 37 Y. Fujimoto, K. Saeki, D. Nakauchi, T. Yanagida, M. Koshimizu, and K. Asai: *Sens. Mater.* **30** (2018) 1577.
- 38 T. Yanagida, M. Sakairi, T. Kato, D. Nakauchi, and N. Kawaguchi: *Appl. Phys. Express* **13** (2020) 016001.
- 39 M. Arai, K. Takahashi, Y. Fujimoto, M. Koshimizu, T. Yanagida, and K. Asai: *Rad. Meas.* **134** (2020) 106328.
- 40 M. Laval, M. Moszyński R. Allemand, E. Cormoreche, P. Guinet, R. Odru, and J. Vacher: *Nucl. Instrum. Methods* **206** (1983) 169.
- 41 D. F. Anderson: *IEEE Trans. Nucl. Sci.* **36** (1989) 137.
- 42 C. W. E. van Eijk: *Nucl. Instrum. Methods Phys. Res., Sect. A* **392** (1997) 285.